Experiments in Fluids 11, 313–324 (1991)

Experiments in Fluids

Counter jet stagnation flows

J. C. Rolon, D. Veynante and **J. P. Martin**

Laboratoire E.M.2.C C.N.R.S. et Ecole Centrale Paris Grande Voie des Vignes F-92290 Châtenay-Malabry, France

F. Durst

Lehrstuhl für Strömungsmechanik Universität Erlangen-Nürnberg Cauerstraße 4 W-8520 Erlangen, Germany

Abstract. The present paper concerns the stagnation flow produced by counter flowing air jets. Little experimental information exists on such flows in spite of their extensive employment in the theoretical treatment of diffusion flames. To remedy this situation, laser-Doppler measurements were performed to quantify the entire flow field. The experiments are described and the results of the velocity measurements presented. Differences between the investigated flow field and the ideal flow field, employed in theoretical studies, are pointed out.

1 Introduction

Two centrally located, opposing jet flows yield a plane stagnation flow region, which is often assumed to be located in the middle plane between the two opposing jet nozzles. Up to date, this assumption was introduced without an experimental proof of the stability of the assumed location. A further assumption made about the flows has been, that its flow field obeys the laws deduced from a potential flow theory yielding the velocity components $u=ar$ and $v=-2az$. If these assumptions are introduced into theoretical treatments of combusting flows, information on combustion can be deduced, and can be compared with experiments to yield information on the "correctness" of the treatment of the chemistry of combustion. However, useful information can only be drawn from such a comparison, if the assumed flow field agrees, to a reasonable extent, with the actually existing flow field. This has so far not been proved for the counter jet stagnation flow.

In recent years, counter flow diffusion flames have gained the increasing attention of scientists and engineers interested in details of the structure of diffusion flames. Karlovitz et al. (1953), Seshadri and Peters (1983), Tam and Ludford (1985) have studied the effect of "flames stretching" on combustion in premixed flames, i.e. the effect of a velocity gradient in the direction of the flame front on the combustion velocity, and they have theoretically deduced from their studies that the burning velocity should decrease if the velocity gradient along the flame front is increased. This result needs to be experimentally verified. For such verifications flames in the stagnation region of two counter jet flows can be employed. Structural changes in the combustion region caused by stretching of flow elements can be looked at and their investigation is strongly facilitated by the particular shape of the flat diffusion flame, e.g. the flame which forms in the stagnation region of two counter flowing jets as sketched in Fig. 1 a.

Detailed structural investigations of diffusion flames and studies of the surrounding flow fields have recently become feasible by means of modern laser diagnostics, i.e. by means of the various molecular laser scattering techniques that are available and by means of laser-Doppler anemometry. In spite of the availability of these techniques, very little detailed experimental information exists on flat diffusion flames or on their flow fields without combustion. In particular, the flow field is not known, i.e. all theoretical studies of flame stretching are based on ideal flow solutions and have

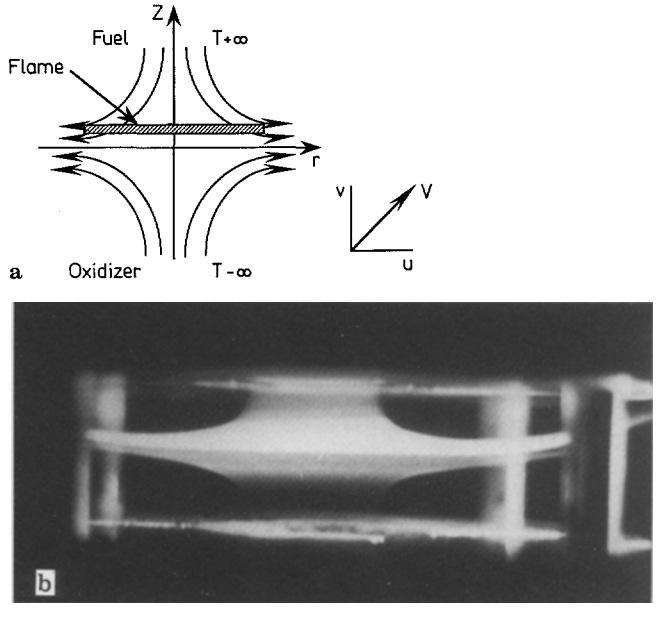

Fig. 1. a Geometry of the flow. The flame is formed in vicinity of a stagnation point established by the counterflows of oxydant and fuel; **b** laser sheet visualisation of the counterflows without flame

not been compared to accurate experimental results. Earliest theoretical treatments, e.g. see Spalding (1961), Fendell (1965), Jones et al. (1972) and Liñan (1974), were based on assumed flow fields derived from potential theory like the ones derived by Leclerc (1950) or Bird et al. (1960). In this way the treatment of flat diffusion flames can be looked at as being a subject where combustion and flow are treated separately from each other neglecting the diffusion of momentum (viscosity) all together. This is in disagreement with the physics of the phenomenon as it is nowadays understood, e.g. Tsuji (1982); suggesting a strong coupling of the diffusion transport of chemical species and momentum. The particle tracking measurements by Pandya and Weinberg (1964), show that the flow patterns of flat diffusion flame is strongly influenced by the heat release from the flat combustion region. It is the long term aim of the present project to study this interaction in detail.

The present paper is concerned with the flow field which establishes itself in the "center region" of two counter flowing jets as they are set up (Fig. 1 b) to produce flat diffusion flames as those shown in Fig. 2a and 2b. Only measurements without combustion are provided. Laser-Doppler measurements are described of axial and radial velocity components with detailed measurements being given in the stagnation plane of the flow. Slightly off this plane, towards the jet that provides the oxygen, the flat flame will establish itself with a distance of approximately 1 to 2 mm away from the stagnation plane. The present measurements show that the flow field in the region where the flame will establish itself, differs from the flow field prescribed in theoretical treatments, i.e. it has properties far different from those of the assumed potential flow field. It is unlikely that combustion will alter the velocity field in such a way that the potential flow field is readily applicable. Because of this the paper strongly suggests to continue research on flat diffusion flames only in conjunction with detailed studies of the flow field in which the flame establishes itself.

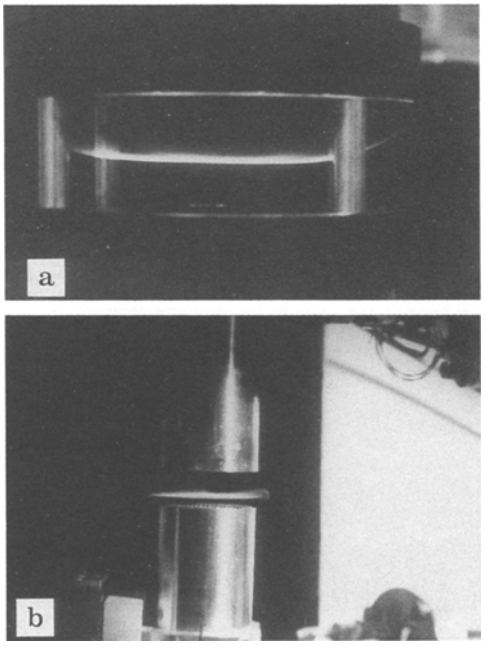

Fig. 2. **a** Flat propane-air flame with burner type I; **b** flat propane-air flame with burner Type II

Due to this lack of experimental data, theoretical treatments (see review papers by Tsuji 1982 or Spalding 1961) are generally based on a potential flow theory description of the flow fields as proposed by Leclerc (1950) or Bird et al. (1960). Combustion and flow are treated separately, neglecting viscosity and heat release effects, which is in disagreement with the physics of the flow (Tsuji 1982). The available theroretical treatments are based on the following assumptions for the flow field:

$$u = ar \quad \text{and} \quad v = -2az$$

which can be deduced from Euler's equations for the counter jet diffusion flame. The quantity a is the strain rate:

$$a = \mathrm{d}u/\mathrm{d}r$$

and is assumed to be a constant.

Spalding (1961) proposed for a the value:

$$a = V_0/D$$

where V_0 is the jet exit velocity and D the jet diameter, whereas Williams (1981) uses:

$$a = 2V_0/H$$

with H the distance between the two burner nozzles.

To validate or disregard these theoretical assumptions, detailed experimental measurements of the flow fields are needed. In the present study, details of the flow field were obtained employing laser-Doppler anemometry and results are presented for various flow settings. Implications to structural properties of flames are given and are also drawn from visualization and photographic records.

Two different jet arrangements were set up corresponding to the Type I and Type II diffusion flame configuration, described by Tsuji (1982). The entire test facility and the two burners are described in Sect. 2. The flow fields of these burners were studied by means of a laser-Doppler anemometer system, described in Sect. 3. Results of the final measurements are given in Sect. 4 and conclusions and final remarks in Sect. 5.

2 Test facility

To carry out detailed flow investigations of counter jet stagnation flows yielding flat diffusion flames, a test facility was set up at E.M2.C Laboratory (CNRS and Ecole Centrale Paris). This facility is shown in Fig. 3 in the form of a block diagram. The figure indicates the two separate flow control lines set up to supply the oxygen and the fuel to the two plenum chambers of the nozzles located opposite to each

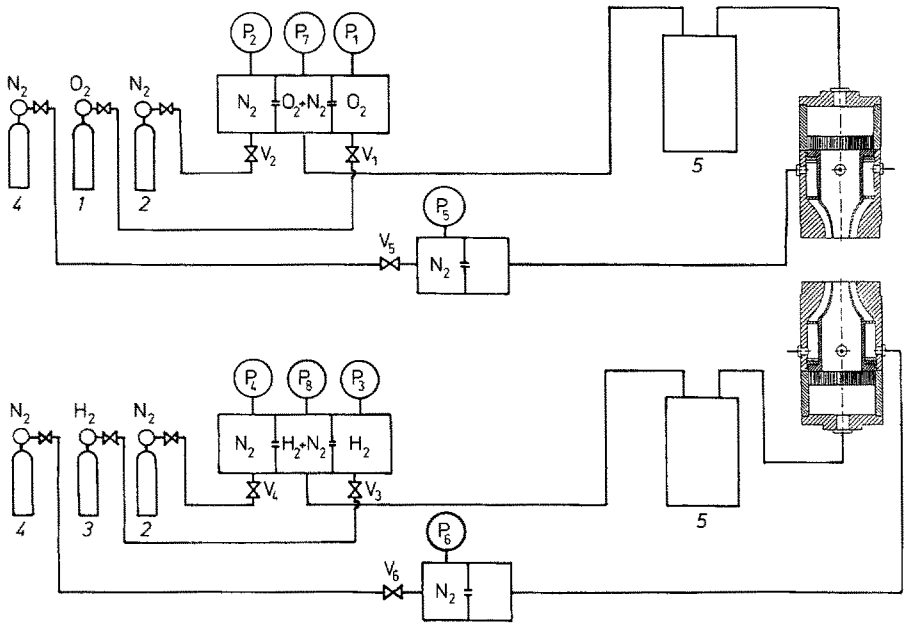

Fig. 3. Flow devices and control. *1* Oxygen supply, *2* Nitrogen supply, *3* Fuel supply, *4* Outer ring flow nitrogen supply, *5* Particle seeders for LDA measurements, P_1, P_8 Pressure captors for flow regulation and controls

other to make up the counter jet stagnation flows. The oxygen and fuel were supplied from compressed oxygen and fuel bottles and H_2, CH_4 and C_3H_8 were usually employed as fuel. In addition, compressed nitrogen was available in bottles for diluting both the oxygen and the fuel. To control the mass flow rates of the gases, pressure regulators in conjunction with minute, chocked, sonic nozzles of 0.2 mm to 1.75 mm in diameter were employed in each of the flow lines. Each line also comprises mixing devices to allow the oxygen and fuel supplies to be diluted and well mixed with N_2 prior to feeding the flow streams through the plenum chambers of the oppositely located nozzles. In this way, well controlled flow and chemical conditions could be adjusted by the set-up flow system for all the studies carried out by the authors.

In order to allow laser-Doppler measurements to be performed in the flow field between the nozzles, both flow streams were seeded with scattering particles using silicon oil particle seeders. The upper size limit of the resultant particle size distribution was approx. 3–4 μm. In this way, seeded gas flow streams resulted that maintained their particles up to the investigated flow region and, hence, yielded conditions well suited for laser-Doppler measurements. It was demonstrated in verification experiments, that the employed particles were sufficient in size for good light scattering and small enough to follow the flow with sufficient accuracy.

In order to obtain information on the flow rates of both gas streams, the pressures before and after the flow controlling sonic nozzles were recorded with the help of piezo resistive transducers. The output voltage of these devices was digitized and recorded with a PDP 11/23 microcomputer. From these pressure records the actual flow rates were computed and, in this way, the flow rates could be monitored throughout the experiments described in this paper. Both streams of the flow were adjusted to provide equal flow momentum out of the two oppositely located burners corresponding to a mean burner exit velocity of 0.6 $m \cdot s^{-1}$. This yielded a total volume rate of 1,060 $l \cdot h^{-1}$. At the outlet, the flow was at the atmospheric pressure and a temperature of close to 23 °C.

Figures 4 and 5 show the two burners that were employed by the authors. They correspond to Type I and Type II burners as defined and introduced by Tsuji (1982). The major dimensions of both burners are given in Figs. 4 and 5 and their mounting within the laser-Doppler anemometer is indicated in Fig. 6.

The Type I burner of Fig. 4 was constructed in such a way that the supplied gas (oxygen or fuel) for the main stream was entered through a central pipe line. It entered a small plenum chambre filled with aluminium wool to allow the flow to settle prior to being passed through honeycomb flow straighteners. The main flow then entered the straight part of the nozzle which had a diameter of $D = 64$ mm. The gas flow was then accelerated through the converging part of the nozzle to have, for the present studies, at the 25 mm in diameter exit a centre outlet velocity of 0.645 $m \cdot s^{-1}$.

The protecting N_2-gas flow was entered into the burner Type I through 4 supply lines, located circumferentially around the burner. The N_2-gas entered a ring like plenum chamber where it was also allowed to settle, before passing a flow straightener and leaving through a ring-like nozzle surrounding the inner nozzle of the main stream. The outer nozzle had an inside diameter of 29 mm and outside diameter of 49 mm. The Type I nozzle burner showed a flat top part providing a 124 mm diameter base as shown in Fig. 4.

The employed matrix burner was constructed differently, see Fig. 5. Each matrix burner consisted of a centrally located supply line through which the main gas flow (oxygen or fuel) was passed to enter a settling chamber with a centre

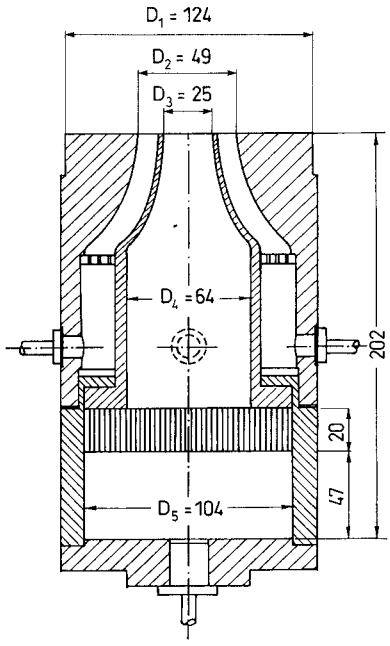

Fig. 4. Sketch of burner type I with detailed dimensions in mm

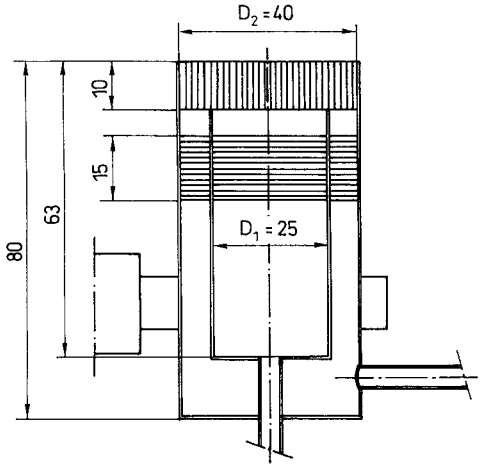

Fig. 5. Sketch of burner type II with detailed dimensions in mm

diameter of 25 mm. From there the flow passed 10 wires meshes with an open area of 35%, mounted behind each other to calm down any disturbances of the incoming flow prior to passing it through a square hole matrix of 10 mm length, 1 mm side opening, and 1 mm wall thickness of the tubing. Out of these tubes, small jet-like flow streams resulted that combined to a main flow out of each of the oppositely located burners. In the stagnation region of the combined flows, the initially jet-like structure of the flow had disappeared leaving a nearly smooth, radially strongly stretched flow.

To protect the flat diffusion flame again from negative effects of the surrounding air, a N_2-gas flow was supplied through a surrounding ring flow. This flow passed also the

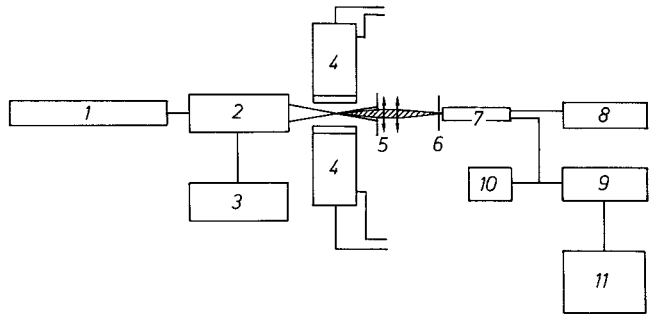

Fig. 6. Sketch of the experimental set-up including LDA system, burners and electronic equipement. *1* He-Ne laser, *2* LDA transmission optic with double Bragg cell, *3* Bragg cell power supply, *4* Burners, *5* Light collecting lens with light stop for the incident laser beams, *6* Pinhole, *7* Photodetector, *8* Photodetector and preamplifier power supply, *9* LDA counter, *10* Oscilloscope, *11* Computer

square hole matrix at the top of the burner, coming from a second surrounding plenum chamber shown in Fig. 5. The flow to this chamber was provided through a side hole and again 10 meshes of 35% opening were used to smooth the flow prior to passing it through the matrix.

To mount the two Type I or Type II burners opposite to each other, special mounting arrangements were employed. These relied on the precision manufacturing of the outside housing of both burners. These sleeves were removed again after the burners were fixed to rigid supports mounted on the main frame of the burner test rig. This frame was mounted on a three-dimensional traversing table for positioning the burner relative to the measuring control volume of the stationary laser-Doppler anemometer employed.

3 LDA-system and velocity measurements

3.1 LDA-equipment and particle seeding

To study the flow field of counter jet stagnation flow yielding flat diffusion flames, a laser-Doppler-anemometer was set up operating with forward scattered light. This forward scattering arrangement is indicated in Fig. 6 which shows the LDA-system and its arrangement relatively to the investigated counter jet stagnation flows. The employed LDA-system consisted of a 15 mW He-Ne-Laser mounted on an optical bench which also acted as a mount of the LDA-transmission optics. This optic consisted of a single channel LDA-system manufactured by OEI-Optoelektronische Instrumente GmbH embracing an integrated optics with beam splitter, double Bragg cell, and focusing lens to guide the two light beams into the measuring volume of the LDA-system. This volume is made up of the two crossing light beams leaving the transmission optics. Particles passing the crossing region scatter light and part of this is collected in the forward direction by the light collecting lens which is facilitated with two light stops for the incident beams so that only

the scattered radiation passes and reaches the photo detector through a pinhole.

All the parts to the optical system were interconnected and mounted in such a way that the optic stayed aligned for one complete set of investigations corresponding to one burner. The LDA optical system was rotatable and allowed measurements of both the vertical and the horizontal velocity components, both being measured independently of each other. The employed high precision rotating mount assured high accuracy of the beam positioning and, hence, also of the location of the measuring position.

In order to perform the laser-Doppler-measurements with frequency shifting, the optical system was facilitated with the necessary electronics to drive the double Bragg cells. Electronics were also available for the laser and the photomultiplier. An oscilloscope was used to watch the signal quality obtained from the photomultiplier and this oscilloscope was also employed to assure that the noise between individual Doppler signals was less than 20 mV in all operations. This was necessary to assure that the electronic frequency processing system worked without noise interfering with the recording of the Doppler bursts.

In order to provide sufficient scattering particles to obtain about 1,000 validated signals per second, two homemade particle seeders were employed consisting of spring jets as sketched in Fig. 7. These particle seeders used the gas-mixture-jet to cause a subpressure at the tip of a suction pipe which entered with its back end into the liquid to be sprayed. At a certain onset jet-velocity, the liquid was sucked up from the container and sprayed to yield the scattering particles needed for laser-Doppler measurements. These were found to be extremely small, i.e. the mean diameter was approximately 1.5 μm, so that they followed the small velocities which characterized the flow field between the burners. Hence, the settling velocity was negligible in comparison to the flow velocity studied.

Silicon oil was employed as spraying liquid, it had a low vapour pressure and ensured that the particles that left the spray generator did not evaporate in the connecting pipes and holes leading the gases to the burner.

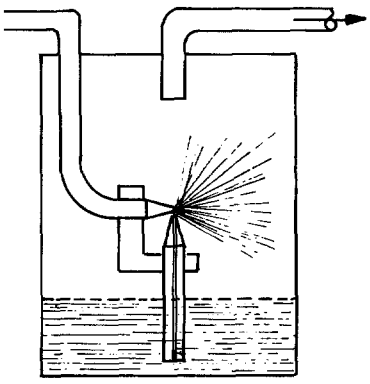

Fig. 7. Spring jet particle seeder

3.2 Electronic signal processing and data acquisition

To yield good electronic signals for processing, the scattered light from the measuring volume was collected by a double lens and focussed onto a pinhole in front of the photomultiplier. The LDA-optical signal was converted into an electrical signal resulting in individual Doppler burst showing signals with amplitudes of 700 mV to 800 mV maximum. These signals were observed on an oscilloscope and were employed for some final adjustments of the location of the photomultiplier pinhole in order to assure good signal quality. Adjustment were made for maximum amplitude, maximum modulation depth and maximum particle number. After this adjustment, the signal was transfered to a DISA-counter, model 55496, which was operated with a band pass filter setting of 64 kHz and 2 MHz. Since the actual Doppler signal frequency was of the order of 200 kHz maximum, and since 200 kHz frequency shift was applied through the Bragg cells, these settings were found to be sufficient to avoid any loss of information and to assure high percentage of signal acceptance. Observing the acceptance rate, the laser light power, the voltage supply to the photomultiplier and the amplifier gain of the counter were complementarily adjusted to yield good signals with a noise level between the signal bursts of approximately 20 mV at the input to the DISA-counter. These signals were available to the actual counter part of the DISA electronics which was operated in the so called combined mode. About 200 to 1,000 validated signals per second were obtained at each measuring point depending on the instruments settings and on the location in the flow. About 2,000 signals contributed to the actual mean values taken as a velocity information and recorded for further evaluation.

The individual counter measurements were supplied to the PDP 11/23 micro-computer which handled the data and computed the actual Doppler frequencies. This computer also controlled the movement of the burner assembly relative to the spatially fixed optical sytem to yield the local velocity distribution of the counter jet flow stagnation flow field. For each measuring point, information regarding the measuring location, the mean velocity, the "turbulence intensity", the mean particle rate, etc. were displayed yielding information that allowed the state of the flow field to be judged and also the required particle rate to be assessed. It was easy to see from the displayed information whether the flow was laminar or presented turbulent fluctuations due to disturbances from the surroundings. If such disturbances were observed, the measuring point was repeated twice and only taken as final information if the two readings agreed within $\pm 2\%$. In this way, reliable measurements could be obtained in the entire flow field and for all flow conditions.

The individual velocity readings were stored together with the measuring location and were finally plotted in form of tables and diagrams. This final information is provided in Sect. 4 and is used for further discussions of the results in Sect. 5.

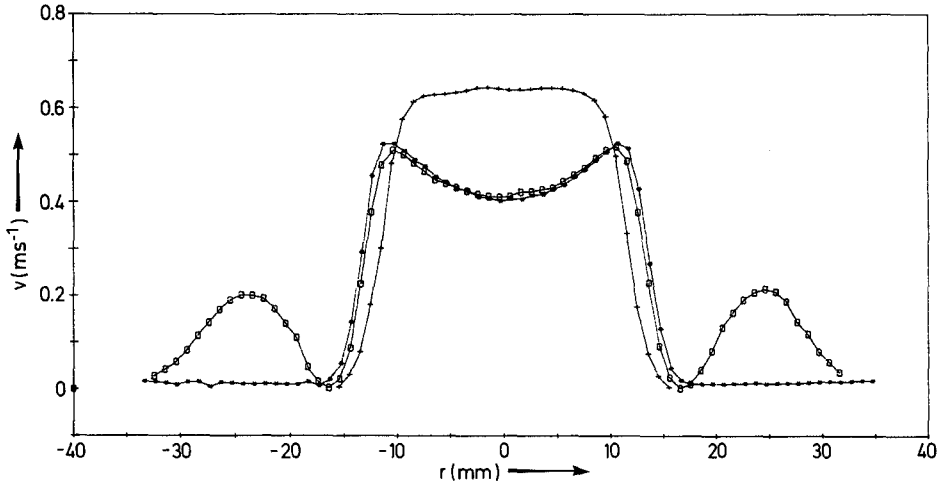

Fig. 8. Axial velocity component, measured at 7.7 mm out of the exit of the nozzle for three cases: (+)–Free jet produced by one nozzle, without opposed jet or surface, and without the surrounding ring flow, (*)–Counter-flow produced by two identical opposed jets without surrounding ring flow, (o)–The surrounding ring flow when present does not modify the central velocity profile

3.3 Velocity measuring procedure

To set up the flow, test measurements were performed prior to the investigations of the velocity field. Each of the two nozzles of burner Type I was investigated on its own by means of the laser-anemometer and the resultant velocity field was compared with the expected field for which the nozzle was designed. Figure 8 shows an example of an axial velocity profile measured just downstream of the nozzle mouth. Last minute adjustments were made to account for imperfections in the velocity distribution at the jet exit and to assure repeatability of the measurements within $\pm 1\%$ at all positions just downstream of the nozzle mouth. For all flow cases, it was also assured prior to measurements that flow symmetry was better than $\pm 2\%$ across the nozzle cross section. When all these conditions were reached, the two nozzles were set up opposite to each other and the flow was adjusted according to the predefined conditions. Some measuring points were rechecked before the center of the jet nozzle was searched for and from this position, velocity profiles were taken in radial area of $+25$ mm. This region was considered the part of the flow to be of major interest. In it the flat flame stabilized and takes on the shape shown in Figs. 2a–2b.

Starting at the center position of the flow, measurements were taken at various distances from the centre between the two burner's top surfaces and various radial positions. For each measuring plane the z-position was selected manually and radial traverses were carried out by an automatic traverse and controlled by the PDP 11/23 computer. Measurements were taken every mm in the radial direction. Following the axis, variable position steps were used, but near the stagnation plane 0.5 mm position steps were selected to resolve the strong velocity gradients occuring in this part of the flow. This spatial resolution was found to be sufficient in order to recover the major features of the flow, even those characterizing the stagnation region of the two counter flowing jets. Particular attention was given to this region in order to see how experimentally obtained velocity distributions agreed with the theoretical flow fields used in the modelling of flat diffusion flames.

In the present set of investigations, the mean velocities at the outlets of the counter flowing jets were equal and constant all over the different test conditions. The distance between the burners was the only parameter varied in the study. In the present paper, experimental results of four test cases are reported. They show the major features of the flow and its dependence on the distance between the front surfaces of the jet producing nozzles. Even when symmetric input flow conditions are set up, asymmetric flows conditions result. The asymmetry of the flow increases with decreasing distance between the burners. One flow case for the Type II burner is also reported to complete the information provided by the present study.

4 Results and discussions

On all the following representations reference point $r=0$, $z=0$ is chosen to be located on the flow axis and at equal distances $H/2$ from the burners (Fig. 1).

4.1 Flow field of burner Type I

The flow field of the burner Type I was extensively investigated and in this paper, the authors report on one set of experimental results for which the burner separation was varied, to provide separations of $H=15$ mm, 25 mm, 28.6 mm and 35 mm. These separations are denoted as Flow Cases 0, I, II and III respectively and they were run for nearly equal outlet conditions, details of which are given in Table I. Under these conditions, the radial (u) and axial (v) velocity components between the burners were obtained and are tabulated to be used for comparison with numerically computed flow fields. Detailed information in tabulated

form is available from the authors. Figures 9 to 15 show diagram presentations of these data which allow particular flow features to be discussed.

4.1.1 Axial velocity profile at the output of the nozzle

In order to test the ability of the jet producing nozzles to give well controlled one dimensional laminar flows the authors first measured the free jets coming out of each nozzle. The jet, produced by one nozzle, flows into the surrounding air, without opposed jet or surface and without the surrounding ring flow. Figure 8 curve 1 (+) shows the axial v velocity component, measured 7.7 mm out of the exit of the nozzle. It shows a very constant central part of the velocity profile as expected.

Table 1. Flow settings for flow cases 0 to III. Choked sonic nozzles of 0.8 mm I.D. were used in pressure regulators: H–Burner separation; P_0–Generating pressure in pressure regulators; $V°$–Volume rate of air; V_0–Air mean outlet velocity of the burners

	H (mm)	P_0 (bar)	$V°$ 10^3 (l/h)	V_0 (m/s)
0	15.0	2.9	1.06	0.60
I	25.0	2.9	1.06	0.60
II	28.6	3.5	1.10	0.62
III	35.0	2.9	1.06	0.60

When the two nozzles were opposed to each other and when the counter flow was produced between the two jets, the velocity profiles, still recorded at 7.7 mm away from the nozzles mouth, changed drastically: the v component was reduced and the u component increased according to mass conservation; at the same time the constant v velocity component region around the flow axis disappeared and a M or W shape profile was observed [see Fig. 8 curve 2 (*)]. One has certainly to take this phenomenon into account for further theoretical work on these flows.

There was also an influence of the surrounding ring flow on the final velocity profile but this influence is negligible as shown by Fig. 8 curve 3(0).

4.1.2 Global representation of the flow field

Figures 9 a and 9 b show a vector representation of the entire flow field obtained for flow case II. They indicate that two different asymmetric stable flows existed even if the same equal momentum condition was set up for each of the oppositely located nozzle outlet flows. A detailed analysis of the flow field showed that if one of the flow fields is imaged at the center line between the burners, the other field results (if the stagnation point of one flow is located at Z_0 the one of the other flow is located at $-Z_0$). Hence it is sufficient to discuss only one of the flow configuration. Just restarting the flow could cause the reversed location of the stagnation plane to occur. The asymmetry can be caused by distur-

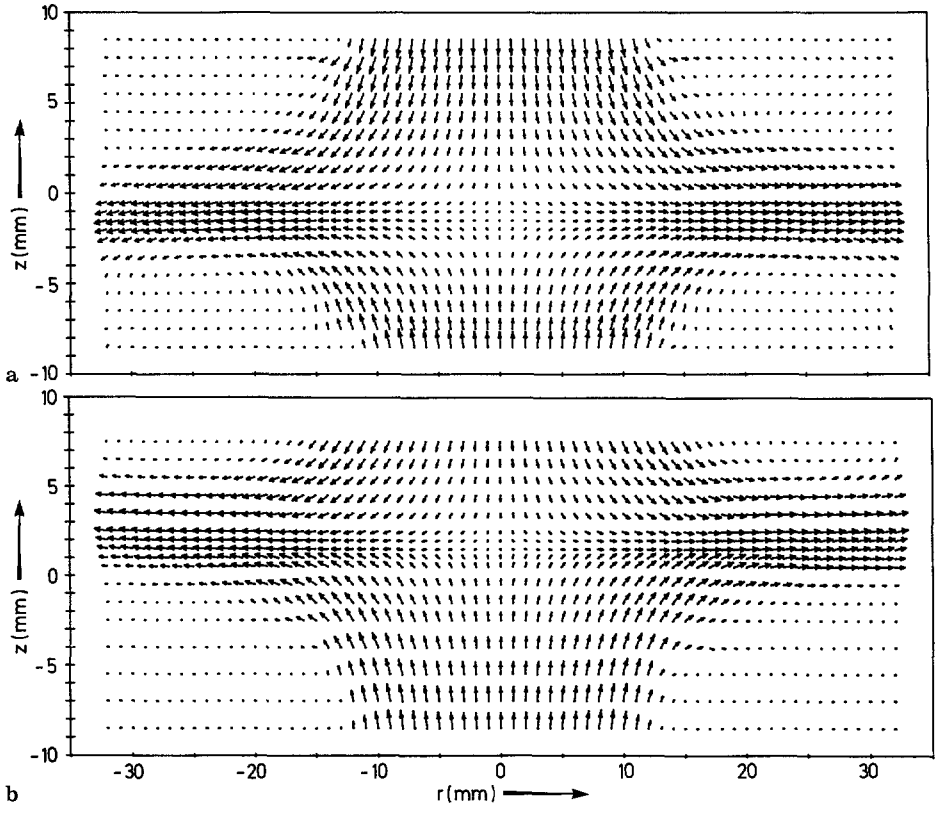

Fig. 9. a Vector representation of the measured flow field or flow case II, with lower position of the stagnation point $Z_0 = -1.5$ mm; **b** vector representation of the measured flow field for flow case II, with upper position of the stagnation point $Z_0 = 1.5$ mm

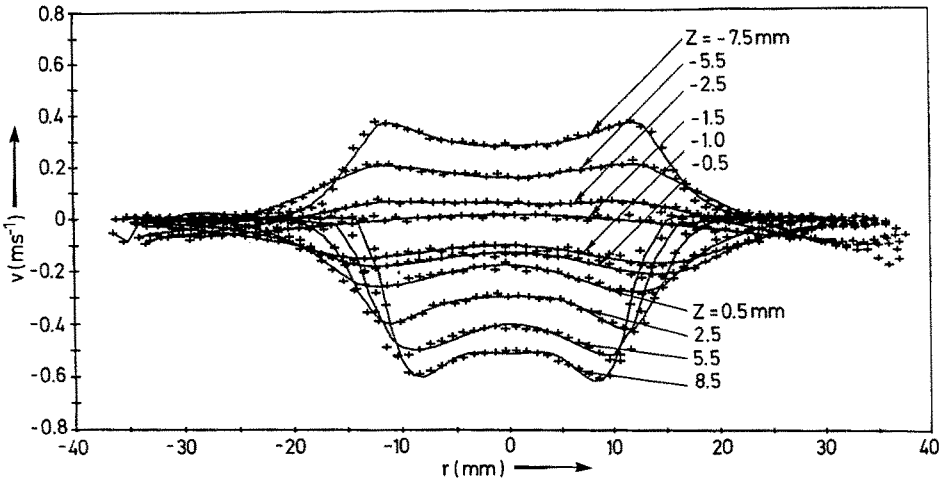

Fig. 10. Radial profiles of the v (axial) component of the velocity field at different z locations

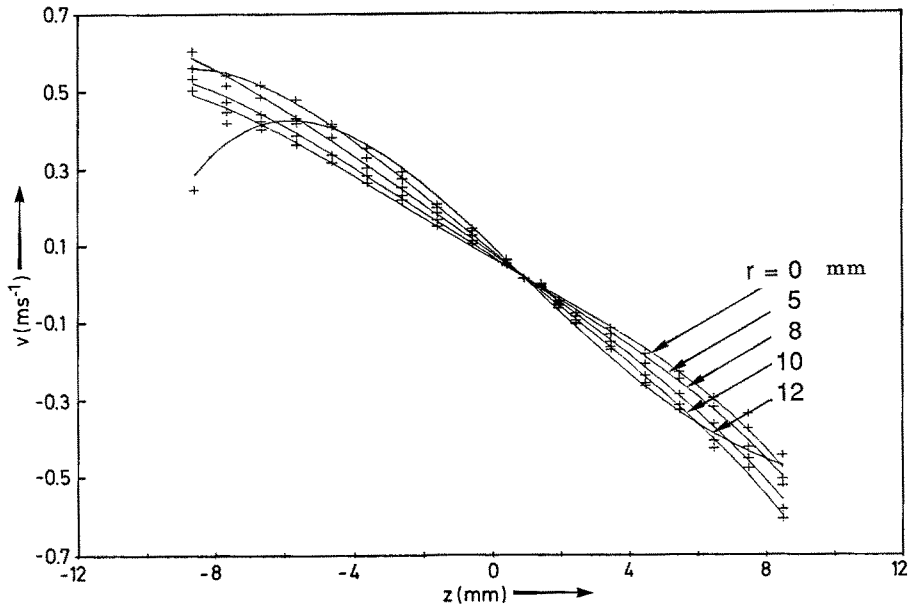

Fig. 11. Axial profiles of the v (axial) component of the velocity field at different r locations

bances and results in recirculating flow regions that establish themselves near the horizontal burner surfaces. The larger of these regions was located further away from the stagnation plane of the flow. The experiments confirmed that recirculating flow regions always form if both nozzle mounths are surrounded by plane surfaces that are positioned at a distance H away from each other. No recirculating flow region exists when the surfaces are removed so that the nozzle mouths finish with wall rings.

4.1.3 Axial component of the velocity

Details of the radial profiles of the v (axial) component of the velocity field at different z locations are provided, for test case II, in Fig. 10. For this flow $Z_0 = 1.5$ mm. In the central flow region (-10 mm $< r < 10$ mm), v decreases from the outlets of the nozzles to the stagnation plane. When approaching Z_0, the M shape of the velocity profile is smoothed and v does not depend too much on r when -1.5 mm $< z - Z_0 < 1.5$ mm.

Figure 11 provides the axial profiles of the v component of the velocity for various r locations. Only profiles in the central part of the flow are provided, and v increases linearly with z. A carefull analysis of the experimental tabulated data, shows that for $r < 3$ mm the slope is constant, noted k_2 in the following sections. Out of the axis, the slop increases slightly with r.

4.1.4 Radial component of the velocity

Figures 12 provide the radial distributions of the u (radial) component of the velocity as a function of r for various z locations. We can divide these curves into three different parts. Around the axis (-7 mm $< r < 7$ *mm*) u increases linearly with r with a characteristic slope, this slope will be noted k_1 for $z = Z_0$; for larger r we observe a second linear

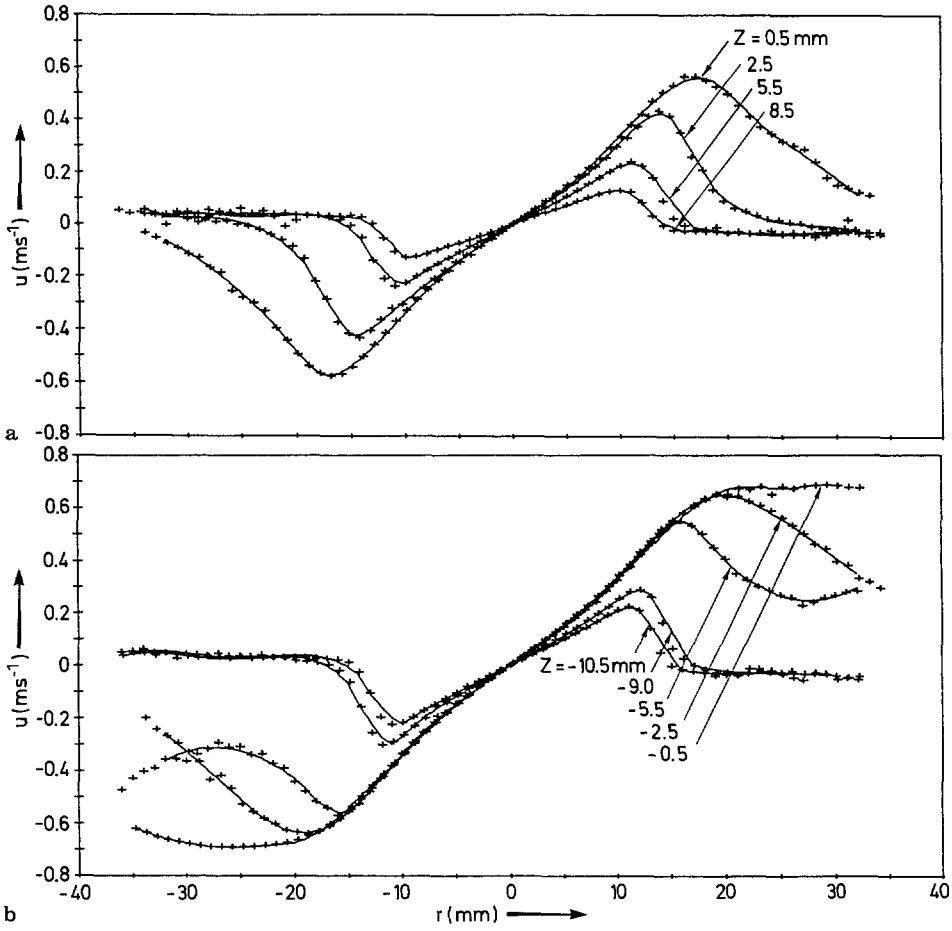

Fig. 12. **a** Radial profiles of the u (radial) component of the velocity field at different z locations; **b** radial profiles of the u (radial) component of the velocity field at different z locations

Table 2. k_1 and k_2 are the mean values for the experimentally determined strain rate; Z_0 is the stagnation point; V_0 is the air mean outlet velocity of the burners; D is the nozzles diameter and H the distance between them

	H (mm)	Z_0 (mm)	k_1 (s^{-1})	k_2 (s^{-1})	V_0/D (s^{-1})	$2V_0/H$ (s^{-1})
0	15.0	0.4	37.0	–	24.0	80.0
I	25.0	−1.4	29.2	27.6	24.0	48.0
II	28.6	1.5	29.0	28.4	24.0	45.7
III	35.0	−2.8	28.6	28.2	24.0	37.4

increase with a larger slope. At a given point (depending on z) u reaches a maximum after which it decreases. For $Z_0-1\text{ mm}<z<Z_0+1\text{ mm}$, the decrease is observed only after a constant u region: this is caused by the stretching in the stagnation plane. Out of this region the stretching is reduced and interaction between the flow and the recirculating zones is more pronounced. In the $Z_0-1\text{ mm}<z<Z_0+1\text{ mm}$ region, the slope is equal to k_1 and independent of z. Further out of the stagnation plane this slope decreases with increasing z.

Figure 13 shows the u distribution as a function of z for various r locations. Around Z_0 and for $-12\text{ mm}<r<12\text{ mm}$, a constant $\partial u/\partial z=0$ region is observed.

4.1.5 Radial evolutions of u and v for various burners separations H flow cases 0, I, II and III

The above described general features of the flow remain valid for all of the 4 flow cases that are not all described in detail. One can draw the same figures as the one shown in Figs. 8 to 13. Of course the Z_0 position of the stagnation plane is different in each of the cases as seen from Table 2. The major and fundamental difference between the flow characteristics is discussed in the following paragraph.

Figures 14 and 15 show the radial distribution of u and the axial evolution of v respectivally for various burners separations H. One can see that the central part slope of each curve depends on H. Thus this shows that k_1 and k_2 are functions of the burner separation. In the centre part of the flow the slope increases with decreasing distance between the burner nozzle outlet planes. On the other hand, the slopes of the v-velocity distributions along the axis of the burner arrangement show relatively constant values, see Fig. 15.

4.2 Flow field of burner Type II

In the present work, the authors have also investigated the flow field of the two opposite Type II matrix burners without

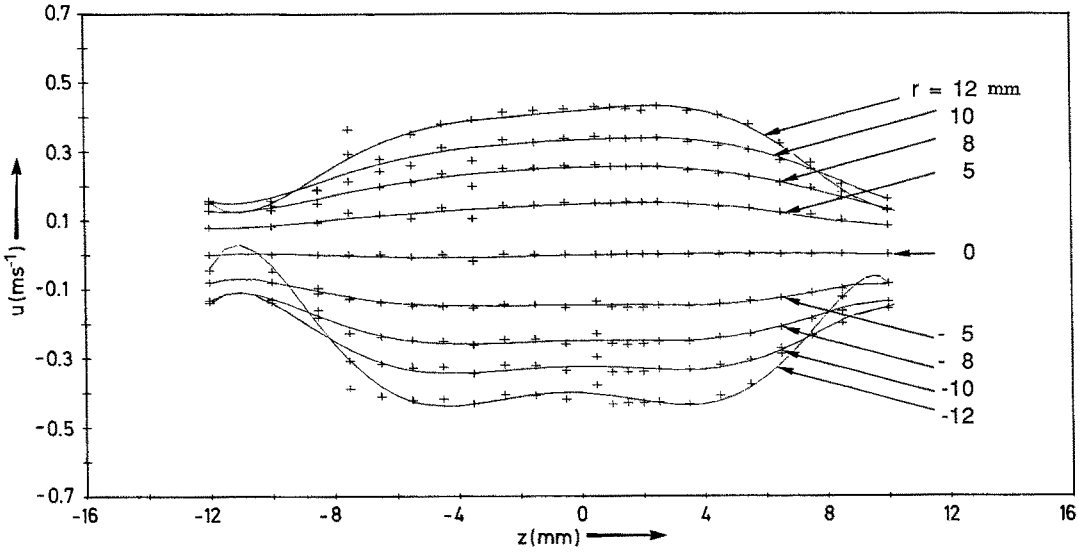

Fig. 13. Axial profiles of the u (radial) component of the velocity field at different r locations

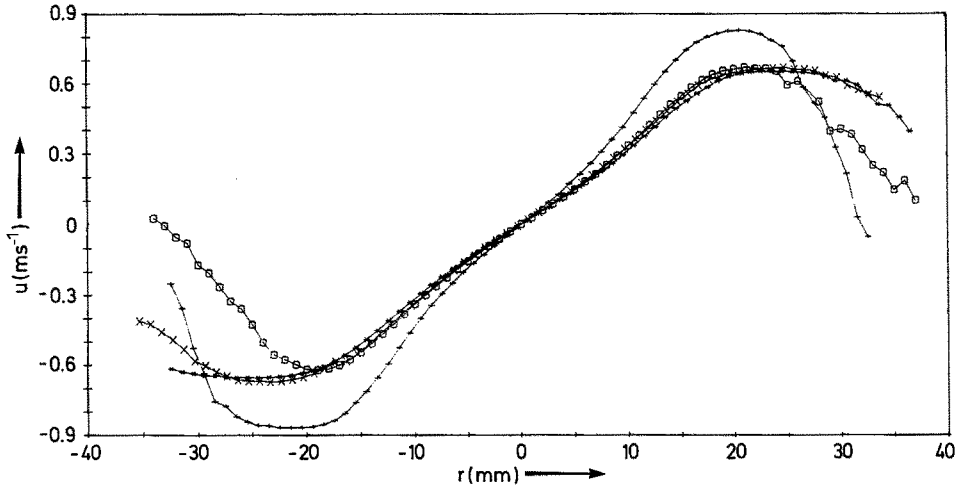

Fig. 14. Radial evolution of the u (radial) component of the velocity for various burners separation H. (+)–$H=15.0$ mm, (o)–$H=25.0$ mm, (×)–$H=28.6$ mm, (*)–$H=35.0$ mm

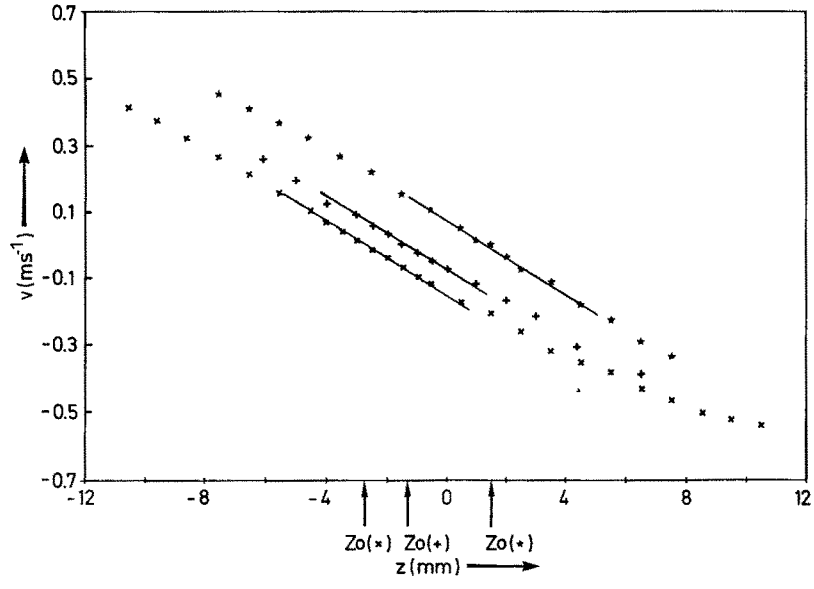

Fig. 15. Axial evolution of the v (axial) component of the velocity for various burners separation H. (*)–$H=28.6$ mmm, (+)–$H=25.0$ mm, (×)–$H=35.0$ mm

combustion. Such burners are easier to build than Type I burners and have been previously used by many authors e.g. Potter and Butler (1959), Pandya and Weinberg (1964), Smooke et al. (1986). In experiments with these burners, the flow is constituted by two counter air streams flowing out of a set of two matrix burners. Again detailed velocity measurements of the flow field produced by this set of burners were carried out and a summary of measurements is provided in Figs. 16 to 18. Figures 16 and 17 show the v component as a function of r at two z locations. These figures indicate that the flow leaves the matrix-burner as small jets that merge into a main flow which afterwards enters the stagnation region between the two burners. At the burner exit (Fig. 16) the v profile is strongly modulated by the wakes of the walls of the matrix channels. These wakes remain apparent in the v component near the stagnation region although the actual velocity profiles are smoothed by the flow straining in this region, (Fig. 17). In spite of this, combustion experiments showed that flat flames are easily stabilized with these burners as shown in Fig. 2b for a propane-air diffusion flame. This phenomenon may be explained by the strong straining of the flow, yielding a flow field in which the u velocity component (Fig. 18) does not exhibit the profile disturbances of the v-component. Heat release effects due to combustion, producing gas expansion certainly strongly contribute to wash out the effect in the stagnation region. This is confirmed by preliminary measurements (not shown here) of the radial velocity profile in the stagnation plane in this flame. In spite of their ability to yield a flat diffusion flame, the flow conditions at the exits of the Type II burners are not well measured because of the jet like structure of the emerging flow, and, accordingly, they are not recommended for theoretical studies of the flow field for flat diffusion flames.

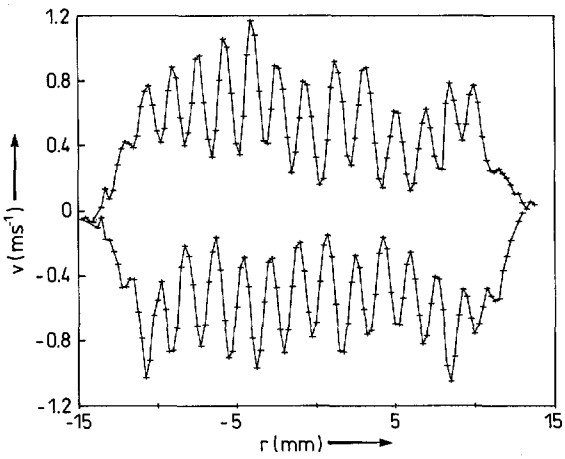

Fig. 16. Radial profiles of the v (axial) component of the velocity measured at $z=-10$ mm and $z=10$ mm from the center for burners type II separation $H=25$ mm

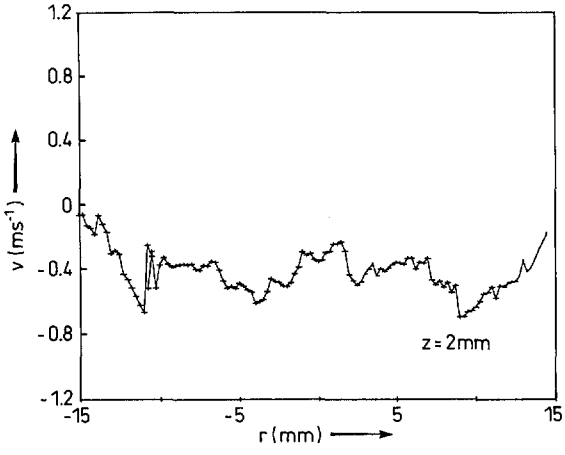

Fig. 17. Radial profiles of the v (axial) component of the velocity measured at $z=-2$ mm from the center for burners type II separation $H=25$ mm

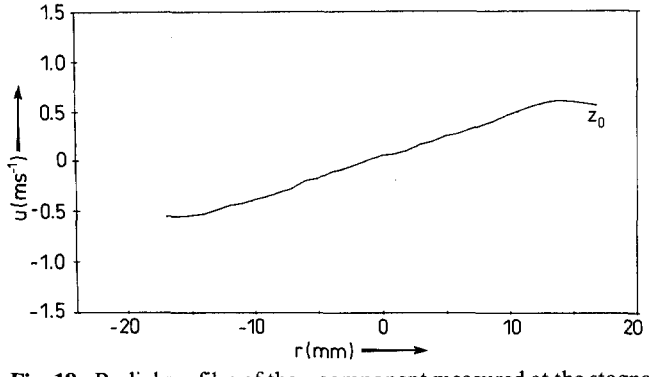

Fig. 18. Radial profiles of the u component measured at the stagnation plane produced by the burner type II

4.3 Comparison between experimental data and theoretical predictions

At various phases of the present experiments, the authors have checked their experimental data for accuracy and consistency. The final data can also be examined to see how well they satisfy the continuity equation. For this purpose, the flow gradient (dv/dz) can be computed by numerically differentiating the measured v-velocity distribution with respect to z and by utilizing the information to check the continuity equation in the following form:

$$r \cdot u = -\int_0^r r \cdot \partial v/\partial z \cdot dr$$

Taking into account, that in the flow region close to the stagnation plane, the two velocity components u and v exhibit linear variations with r and z, respectively, the above equation can easily be integrated to yield:

$$r \cdot u = k_2 \cdot r^2 \quad \text{with} \quad \partial v/\partial z = -2 \cdot k_2$$

Comparing the experimental data via this equation shows that the continuity equation is satisfied in the centre part of the flow to better than $\pm 1\%$. Similar agreement was observed if the continuity equation was verified in the following form:

$$\int_0^\xi \partial u/\partial r \cdot dz + \int_0^\xi u/r \cdot dr = v$$

where ξ was the coordinate in the z-direction with the origin in the stagnation plane. Introducing again

$k_1 = \partial u/\partial r \quad v = 2 \cdot k_1 \cdot z$

In Table 2 the data for k_1 and k_2 are presented together with theoretical data proposed by Spalding (1961) and Williams (1981) for the constant strain rate deduced from a potential solution for the counter flowing jet flow. Small differences exist between k_1 and k_2 reflecting small errors of $\pm 1\%$ in the measurements. The data show, however, that the theoretical value of the strain rate proposed by Williams is notably higher than the experimental results. The value imposed by Spalding (1961) is independant of the distance H and underestimate the experimental value by about 20%. Nevertheless, it seems that the experimentally found k_1 and k_2 values approach the theoretical value by Spalding when H increases, thus the flow field approaches the potential flow solution if the two opposing nozzles are far away from each other.

Considering flow solutions for the counter jet stagnation flow that takes the viscosity of the flow into account, e.g. see Rosenhead (1966), suggest that the flow field can be written as:

$u = k \cdot r \cdot f(\xi)$ and $v = -2(k\,\nu)^{1/2} \cdot f(\xi)$

where k is a constant, ν is the kinetic viscosity and $\xi = z \cdot (k/\nu)^{1/2}$. This solution yields, however, in the centre part of the flow the same gradients as those calculated by the potential flow theory.

The findings summarized in Table 2 readily suggest that the discrepancy between the experimentally found slope of the velocity profile in the centre of the stagnation plane and the theoretical results is entirely due to the choice of small values of H/D in the experiments. To demonstrate this, a test case was run for $H = 15$ mm and the results in Fig. 14 and Table 2 show that the slope increases even faster. This readily suggests that the theoretically found central slope of the velocity profiles is only reached by the experiment for large values of H/D. The present test section did not permit smaller distances to be set up.

5 Conclusions and final remarks

The present paper describes an experimental study of counter jet flows usually employed to yield flat diffusion flames. The experience gained in the present study suggests that quantitative experimental studies of such flows should only employ non-intrusive measuring techniques to avoid intrusion and solve flow disturbances. Laser-Doppler anemometry is well adapted to investigate such flows and it can provide flow details that are not readily available through theoretical studies. As shown in the paper, analytical flow solutions are available, but these capture only the essential features of the flow in the centre of the stagnation plane and yield correct velocity information for large burner separation only. Theoretical studies of combustion in this flow region should be aware of the discrepancy between the analytical and experimental flow field.

Advancements in numerical fluid mechanics and availability of larger computers permit counter jet flows to be predicted. The data provided in this paper might be a good basis for detailed comparisons with numerical results. If good agreement is obtained, the computer program can be extended to also include prediction of combustion processes.

Acknowledgements

The present paper emerged from a collaboration of the author's two laboratories in the fields of fluid mechanics and combustion. The experiments were supported by an E.E.C.-contract ST2J-0273-C (EDB) and the exchange of scientists received support through travel grants within the PROCOPE-Program. Both supports are thankfully acknowledged. The authors also appreciated the help of Dipl. Ing. Döneland in builiding the burner nozzles. Fruitfull discussions with S. Candel and E. Esposito very much stimulated the completion of the manuscript in its present form.

References

Bird, R. B.; Stewart, N. E.; Lightfoot, F. N. 1960: Transport phenomena. New York: Wiley

Fendell, F. E. 1965: Ignition and extinction in combustion of initially unmixed reactants. J. Fluid. Mech. 21, 281–303

Jones, F. L.; Becker, P. M.; Heinsohn, R. J. 1972: A mathematical model of the opposed-jet diffusion flame: Effect of an electric field on concentration and temperature profiles. Combustion Flame 19, 351–362

Karlovitz, Z. B., Dennison, D. W.; Knapschaefer, D. H.; Wells, F. E. 1953: Studies on turbulent flames, fourth international symposium on combustion, Baltimore, Williams and Wilkies, 613–620

Leclerc, A. 1950: Déviation d'un jet liquide par une plaque normale à son axe. La Houille Blanche 6, 3–8

Linan, A. 1974: The asymptotic structure of counterflow diffusion flames for a large activation energies. Acta Astronautica 1001–1009

Pandya, T. P.; Weinberg, F. J. 1964: The structure of flat. Counterflow diffusion flames. Proc. Roy. Soc., A 279, 544–561

Potter Jr., A. E., Buttler, J. N. 1959: A novel combustion measurements based on the extinguishment of diffusion flames. ARS J. 29, 54–56

Rosenhead, L. 1966: Laminar boundary layers, Oxford-clarendon press, 155

Seshadri, K.; Peters, N. 1983: The influence of stretch on a premixed flame with two steps kinetics. Combustion Science Technol. 33, 35–63

Smooke, M. D.; Puri, I. K.; Seshadri, K. 1986: A comparison between numerical calculation and experimental measurements of the structure of counterflow diffusion flame burning diluted methane in diluted air, twenty-first symposium (international) on combustion, Reinhold, New York

Spalding, D. B. 1961: Theory of mixing and chemical reaction in the opposed-jet diffusion flame. J. Amer. Rocket Soc., 3, 763–771

Tam, R.; Ludford, G. S. S. 1985: The stretch-resistant flames of Seshadri and Peters. Combustion Science and Technol. 43, 227–249

Tsuji, H. 1982: Counterflow diffusion flames. Prog. Energy Combustion Science 8, 93–119

Williams, F. A. 1981: A review of flames extinction. Fire Safity J. 3, 163–175

Received December 7, 1990